Chain Length Dependence and Sensing Capabilities of the Localized Surface Plasmon Resonance of Silver Nanoparticles Chemically Modified with Alkanethiol Self-Assembled Monolayers

Michelle Duval Malinsky, K. Lance Kelly, George C. Schatz,*,† and Richard P. Van Duyne*,‡

Contribution from the Department of Chemistry, Northwestern University, Evanston, Illinois 60208-3113

Received September 8, 2000

Abstract: In this paper, we explore the optical properties of Ag nanoparticles chemically modified with alkanethiol self-assembled monolayers (SAMs) by measuring the localized surface plasmon resonance (LSPR) spectrum using UV−vis extinction spectroscopy. For all the experiments presented here, the Ag nanoparticles were fabricated using the technique of nanosphere lithography (NSL) and had in-plane widths of 100 nm and out-of-plane heights of 50 nm. We first demonstrate that unmodified nanoparticles are extremely susceptible to slight changes in 3-dimensional structure when exposed to various solvents. These structural effects can have dramatic effects on the extinction maximum, λ_{max}, of the LSPR shifting it to the blue by over 100 nm. The significant discovery reported here is that λ_{max} for NSL fabricated Ag nanoparticles is extremely sensitive to the SAM properties. We will demonstrate the following new features: (1) λ_{max} of the LSPR linearly shifts to the red 3 nm for every carbon atom in the alkane chain; (2) spectral shifts as large as 40 nm are caused by only 60 000 alkanethiol molecules per nanoparticle, which corresponds to only 100 zmol of adsorbate; and (3) the nanoparticles' sensitivity to bulk external environment is only attenuated by 20% when the nanoparticles are modified with the longest chain alkanethiol (1-hexadecanethiol, ∼2 nm). Experimental extinction spectra were modeled by using Mie theory for Ag nanospheres with dielectric shells intended to mimic the self-assembled monolayer (SAM) in thickness and refractive index. We find that the Mie theory qualitatively predicts the experimentally observed trend that λ_{max} linearly shifts to the red with respect to shell thickness, or alkanethiol chain length; however, the theory underestimates the sensitivity by approximately a factor of 4. Excellent correlation between theory and experiment was observed when Mie theory was used to predict the degree of attenuation in LSPR sensitivity to bulk external environment when the nanoparticle is encapsulated in a dielectric shell similar to an alkanethiol SAM. Finally, we demonstrate that Ag nanoparticles modified with functionalized SAMs can be used in sensing applications. Here, we show that the LSPR shifts to the red 5 nm with the adsorption of the polypeptide poly-L-lysine (PL) to Ag nanoparticles modified with deprotonated carboxylate groups from 11-mercaptoundecanoic acid (11-MUA). Furthermore, we will show that this system behaves reversibly and exhibits no detectable nonspecific binding.

I. Introduction

Currently, there is intense interest in the optical properties of noble metal nanoparticles. This is due, in part, to their use as functional materials in applications including but not limited to the following: optical devices,[1,2] optical energy transport,[3−6] near field scanning optical microscopy (NSOM),[7−11] surface-enhanced spectroscopies,[12−20] and chemical and biological sensors.[21−24] Characteristically, noble metal nanoparticles exhibit a strong absorption band that is not present in the spectrum of

* To whom correspondence should be addressed.
† E-mail: schatz@chem.nwu.edu.
‡ E-mail: vanduyne@chem.nwu.edu.

(1) Dirix, Y.; Bastiaansen, C.; Caseri, W.; Smith, P. *Adv. Mater.* **1999**, *11*, 223−227.
(2) Kroschwitz, J. I.; Howe-Grant, M. *Glass*, 4th ed.; Kroschwitz, J. I., Howe-Grant, M., Eds.; John Wiley & Sons: New York, 1994; Vol. 12, pp 569−571.
(3) Quinten, M.; Leitner, A.; Krenn, J. R.; Aussenegg, F. R. *Opt. Lett.* **1998**, *23*, 1331−1333.
(4) Krenn, J. R.; Dereux, A.; Weeber, J. C.; Bourillot, E.; Lacroute, Y.; Goudonnet, J. P. *Phys. Rev. Lett.* **1999**, *82*, 2590−2593.
(5) Ebbesen, T. W.; Lezec, H. J.; Ghaemi, H. F.; Thio, T.; Wolff, P. A. *Nature* **1998**, *391*, 667−669.
(6) Pendry, J. B. *Science* **1999**, *285*, 1687−1688.
(7) Sánchez, E. J.; Novotny, L.; Xie, X. S. *Phys. Rev. Lett.* **1999**, *82*, 4014−4017.
(8) Knoll, B.; Kellmann, F. *Nature* **1999**, *399*, 134−137.
(9) Hamann, H. F.; Gallagher, A.; Nesbitt, D. J. *Appl. Phys. Lett.* **1998**, *73*, 1469−1471.
(10) Novotny, L.; Bian, R. X.; Xie, S. *Phys. Rev. Lett.* **1997**, *79*, 645−648.
(11) Pufall, M. R.; Berger, A.; Schultz, S. *J. Appl. Phys.* **1997**, *81*, 5689−5691.
(12) Jensen, T. R.; Van Duyne, R. P.; Johnson, S. A.; Maroni, V. A. *Appl. Spectrosc.* **2000**, *54*, 371−377.
(13) Wadayama, T.; Suzuki, O.; Takeuchi, K.; Seki, H.; Tanabe, T.; Suzuki, Y.; Hatta, A. *Appl. Phys. A* **1999**, *69*, 77−80.
(14) Tarcha, P. J.; DeSaja-Gonzalez, J.; Rodriguez-Llorente, S.; Aroca, R. *Appl. Spectrosc.* **1999**, *53*, 43−48.
(15) Emory, S. R.; Nie, S. *J. Phys. Chem. B* **1998**, *102*, 493−497.
(16) Nie, S.; Emory, S. R. *Science* **1997**, *275*, 1102−1106.
(17) Yang, W. H.; Hulteen, J. C.; Schatz, G. C.; Van Duyne, R. P. *J. Chem. Phys.* **1996**, *104*, 4313−4323.
(18) Freeman, R. G.; Grabar, K. C.; Allison, K. J.; Bright, R. M.; Davis, J. A.; Guthrie, A. P.; Hommer, M. B.; Jackson, M. A.; Smith, P. C.; Walter, D. G.; Natan, M. J. *Science* **1995**, *267*, 1629−1632.
(19) Pipino, A. C. R.; Schatz, G. C.; Van Duyne, R. P. *Phys. Rev. B* **1996**, *53*, 4162−4169.
(20) Van Duyne, R. P.; Hulteen, J. C.; Treichel, D. A. *J. Chem. Phys.* **1993**, *99*, 2101−2115.

10.1021/ja003312a CCC: $20.00
Published on Web 01/30/2001

the bulk metal. This absorption band results when the incident photon frequency is resonant with the collective oscillation of the conduction electrons and is known as the localized surface plasmon resonance (LSPR). Along with wavelength selective photon absorption and scattering, LSPR excitation produces enhanced local electromagnetic fields near the surface of the nanoparticle. These electromagnetic fields are responsible for the intense signals observed in all surface-enhanced spectroscopies. The resonance frequency of the LSPR is highly dependent upon the size, shape, dielectric properties, and local environment of the nanoparticle.[25]

Similarly, self-assembled monolayers (SAMs) are also of great general interest for the creation of new functional materials. The most studied classes of SAMs include alkanethiols on Au or Ag and organosilanes on oxides. The attraction of these types of SAMs is 2-fold: (1) they form dense, well-ordered, tightly bonded films and (2) they provide a simple motif for selective tailoring of surface chemical properties. These features are important to many areas of scientific study including molecular electronics,[26−29] biomimetics,[30] lithography,[31,32] sensors,[33−35] corrosion, and nanoscopic tethering agents.[18,28,36,37] Extending this surface-modification technique to nanoparticle systems is an important goal in current materials research since the ability to create nanoparticles with versatile surface chemistry will have significant potential in the applications described above.

To date, much of the work on SAM-modified nanoparticles has been on the synthesis and characterization of small Au nanoparticles in the 1−7 nm size regime modified with alkanethiols,[38−47] ω-functionalized alkanethiols,[48−50] or other thiol derivatives.[51,52] All of the examples listed above were prepared by using a variation of the method developed by Brust et al.[38] which involves a two-phase aqueous−organic system. Modified Au nanoparticles synthesized via this technique have several desirable features. These nanoparticles are stabilized by the chemisorbed thiol capping layer and are readily prepared in large quantities. The size of the Au cluster core can be manipulated by varying the Au:thiol ratio during synthesis.[44] Such nanoparticles act in much the same way as simple chemical compounds in that they can be precipitated, redissolved, and chromatographed without loss of function.[38] However, one of the most significant disadvantages of this synthetic route is the narrow size range over which these nanoparticles can be prepared. This narrow size range prevents full exploitation of their size-dependent material properties for technological applications.

SAMs have also been used as linker molecules in attaching nanoparticles to bulk surfaces or to other nanoparticles creating new types of macroscopic materials.[18,37,53−62] Materials composed of nanoparticle constituents are of great interest because they display useful properties in spectroscopy[18,53] and sensor applications.[37] Similarly, SAMs have been utilized to grow encapsulation layers on nanoparticle surfaces. These types of nanoparticles, commonly referred to as core−shell particles, primarily consist of metal cores with dielectric shells (usually silica or polymer) or vice versa.[63−66] Independent manipulation

(21) Bauer, G.; Pittner, F.; Schalkhammer, T. *Mikrochim. Acta* **1999**, *131*, 107−114.
(22) Storhoff, J. J.; Elghanian, R.; Mucic, R. C.; Mirkin, C. A.; Letsinger, R. L. *J. Am. Chem. Soc.* **1998**, *120*, 1959−1964.
(23) Elghanian, R.; Storhoff, J. J.; Mucic, R. C.; Letsinger, R. L.; Mirkin, C. A. *Science* **1997**, *277*, 1078−1081.
(24) Kreibig, U.; Gartz, M.; Hilger, A. *Ber. Bunsen-Ges. Phys. Chem.* **1997**, *101*, 1593−1604.
(25) Kreibig, U.; Vollmer, M. *Optical Properties of Metal Clusters*; Springer-Verlag: Heidelberg, Germany, 1995; Vol. 25.
(26) Mirkin, C. A.; Ratner, M. A. *Annu. Rev. Phys. Chem.* **1992**, *43*, 719−754.
(27) Rampi, M. A.; Schueller, O. J. A.; Whitesides, G. M. *Appl. Phys. Lett.* **1998**, *72*, 1781−1783.
(28) Klein, D. L.; Roth, R.; Lim, A. K. L.; Alivisatos, A. P.; McEuen, P. L. *Nature* **1997**, *389*, 699−701.
(29) Bumm, L. A.; Arnold, J. J.; Cygan, M. T.; Dunbar, T. D.; Burgin, T. P.; Jones, L., II; Allara, D. L.; Tour, J. M.; Weiss *Science* **1996**, *271*, 1705−1707.
(30) Mrksich, M.; Whitesides, G. M. *Using Self-Assembled Monolayers to Understand the Interactions of Man-made Surfaces with Proteins and Cells*; Stroud, R. M., Hubbell, W. L., Olson, W. K., Sheetz, M. P., Eds.; Annual Reviews Inc.: Palo Alto, CA, 1996; Vol. 25, pp 55−78.
(31) Piner, R. D.; Zhu, J.; Xu, F.; Hong, S.; Mirkin, C. A. *Science* **1999**, *283*, 661−663.
(32) Kumar, A.; Biebuyck, H. A.; Abbott, N. L.; Whitesides, G. M. *J. Am. Chem. Soc.* **1992**, *114*, 9188−9189.
(33) Sackmann, E. *Science* **1996**, *271*, 43−48.
(34) Schuck, P. *Annu. Rev. Biophys. Biomol. Struct.* **1997**, *26*, 541−566.
(35) Knoll, W.; Liley, M.; Piscevic, D.; Spinke, J.; Tarlov, M. J. *Adv. Biophys.* **1997**, *34*, 231−251.
(36) Boal, A. K.; Ilhan, F.; DeRouchey, J. E.; Thurn-Albrecht, T.; Russell, T. P.; Rotello, V. M. *Nature* **2000**, *404*, 746−748.
(37) Mucic, R. C.; Storhoff, J. J.; Letsinger, R. L.; Mirkin, C. A. *Nature* **1996**, *382*, 607−609.
(38) Brust, M.; Walker, M.; Bethell, D.; Schiffrin, D. J.; Whyman, R. *J. Chem. Soc., Chem. Commun.* **1994**, 801−802.
(39) Badia, A.; Gao, W.; Singh, S.; Demers, L.; Cuccia, L.; Reven, L. *Langmuir* **1996**, *12*, 1262−1269.
(40) Badia, A.; Cuccia, L.; Demers, L.; Morin, F.; Lennox, R. B. *J. Am. Chem. Soc.* **1997**, *119*, 2682−2692.
(41) Terrill, R. H.; Postlethwaite, T. A.; Chen, C. H.; Poon, C.-D.; Terzis, A.; Chen, A.; Hutchison, J. E.; Clark, M. R.; Wignall, G.; Londono, J. D.; Superfine, R.; Falvo, M.; Johnson, C. S., Jr.; Samulski, E. T.; Murray, R. W. *J. Am. Chem. Soc.* **1995**, *117*, 12537−13548.
(42) Leff, D. V.; Ohara, P. C.; Heath, J. R.; Gelbart, W. M. *J. Phys. Chem.* **1995**, *99*, 7036−7041.
(43) Hostetler, M. J.; Stokes, J. J.; Murray, R. W. *Langmuir* **1996**, *12*, 3604−3612.
(44) Hostetler, M. J.; Wingate, J. E.; Chuan-Jian, Z.; Harris, J. E.; Vachet, R. W.; Clark, M. R.; Londono, J. D.; Green, S. J.; Stokes, J. J.; Wignall, G. D.; Glish, G. L.; Porter, M. D.; Evans, N. D.; Murray, R. W. *Langmuir* **1998**, *14*, 17−30.
(45) Alvarez, M. M.; Khoury, J. T.; Schaaff, T. G.; Shafigullin, M. N.; Vezmar, I.; Whetten, R. L. *J. Phys. Chem. B* **1997**, *101*, 3706−3712.
(46) Luedtke, W. D.; Landman, U. *J. Phys. Chem.* **1996**, *100*, 13323−13329.
(47) Luedtke, W. D.; Landman, U. *J. Phys. Chem. B* **1998**, *102*, 6566−6572.
(48) Hostetler, M. J.; Green, S. J.; Stokes, J. J.; Murray, R. W. *J. Am. Chem. Soc.* **1996**, *118*, 4212−4213.
(49) Leff, D. V.; Brandt, L.; Heath, J. R. *Langmuir* **1996**, *12*, 4723−4730.
(50) Ingram, R. S.; Hostetler, M. J.; Murray, R. W. *J. Am. Chem. Soc.* **1997**, *119*, 9175−9178.
(51) Johnson, S. R.; Evans, S. D.; Brydson, R. *Langmuir* **1998**, *14*, 6639−6647.
(52) Evans, S. D.; Johnson, S. R.; Ringsdorf, H.; Williams, L. M.; Wolf, H. *Langmuir* **1998**, *14*, 6436−6440.
(53) Bright, R. M.; Musick, M. D.; Natan, M. J. *Langmuir* **1998**, *14*, 5695−5701.
(54) Brust, M.; Bethell, D.; Schiffrin, D. J.; Kiely, C. J. *Adv. Mater.* **1995**, *7*, 795−797.
(55) Brust, M.; Bethell, D.; Kiely, C. J.; Schiffrin, D. J. *Langmuir* **1998**, *14*, 5425−5429.
(56) Mucic, R. C.; Storhoff, J. J.; Mirkin, C. A.; Letsinger, R. L. *J. Am. Chem. Soc.* **1998**, *120*, 12674−12675.
(57) Alivisatos, A. P.; Johnsson, K. P.; Peng, X.; Wilson, T. E.; Loweth, C. J.; Bruchez, M. P., Jr.; Schultz, P. G. *Nature* **1996**, *382*, 609−611.
(58) Colvin, V. L.; Goldstein, A. N.; Alivisatos, A. P. *J. Am. Chem. Soc.* **1992**, *114*, 5221−5230.
(59) Vossmeyer, T.; DeIonno, E.; Heath, J. R. *Angew. Chem., Int. Ed. Engl.* **1997**, *36*, 1080−1083.
(60) Sato, T.; Hasko, D. G.; Ahmed, H. *J. Vac. Sci. Technol. B* **1997**, *15*, 45−48.
(61) Sarathy, K. V.; Thomas, P. J.; Kulkarni, G. U.; Rao, C. N. R. *J. Phys. Chem. B* **1999**, *103*, 399−401.
(62) Resch, R.; Baur, C.; Bugacov, A.; Koel, B. E.; Echternach, P. M.; Madhukar, A.; Montoya, N.; Requicha, A. A.; Will, P. *J. Phys. Chem. B* **1999**, *103*, 3647−3650.
(63) Liz-Marzán, L. M.; Giersig, M.; Mulvaney, P. *Langmuir* **1996**, *12*, 4329−4335.
(64) Westcott, S. L.; Oldenburg, S. J.; Lee, T. R.; Halas, N. J. *Langmuir* **1998**, *14*, 5396−5401.

of the core and shell composition provides a way to engineer optical functionality. Encapsulation of the particle core with an appropriate shell material also offers a means of protection from the surrounding environment.

Although much work has been reported describing the synthesis and characterization of SAM-modified nanoparticles, few investigations have included detailed studies of the optical properties. Because the preparation by Brust et al.[38] incorporates the SAM-modification process during the nanoparticle synthesis, the SAM contribution to the optical spectra of these systems cannot readily be isolated. Whitesides and co-workers[67] presented a study where the optical contribution of SAMs to Au nanoparticles was investigated. In this paper, 40 nm diameter Au nanoparticles were synthesized via citrate reduction of tetrachloroauric acid in aqueous media and then subsequently modified with alkanethiol derivatives. Colloids prepared via chemical reduction characteristically have anions adsorbed to the surface of the nanoparticle. The resulting negative surface charges provide the repulsive forces between the particles that keep them suspended in solution. SAM molecules displace the surface anions disrupting the repulsive forces. This causes the interparticle spacing to decrease resulting in nanoparticle aggregation. Hence, all changes in optical spectra in this study were attributed to aggregation and not to the presence of the thiol capping layer. Aggregation is also responsible for the color changes observed when Au nanoparticles modified with complementary single strands of thiol-DNA are allowed to hybridize.[37] In this system, aggregation can be reversed by melting the DNA to disrupt the Watson and Crick base pairs holding the nanoparticles together. Similarly, Sastry et al.[68] reported significant changes in the optical extinction spectra when Ag and Au colloids modified with thiol-biotin were incubated with avidin. Again, optical changes were attributed to particle aggregation and not to surface modification with the thiol. A few studies by this same group have reported shifts in optical spectra upon formation of thiol-capping layers on Ag nanoparticles.[69,70] Because this observation was not the focus of their investigations, no extensive discussion or explanation of the shifts was included.

In previous studies, we have shown that nanosphere lithography (NSL) is a simple, inexpensive, extremely versatile technique for the fabrication of nanoparticles with controlled size, shape, and spacing that exhibit strong LSPRs.[71−74] Briefly, this technique involves drop-coating a suspension of size-monodisperse polystyrene nanospheres of diameter D onto a substrate where they spontaneously form a hexagonally close-packed monolayer. The monolayer of nanospheres then acts as a deposition mask through which a material, usually a metal, is deposited via thermal evaporation, pulsed laser deposition, or e-beam deposition to a controlled mass-thickness, d_m. After deposition, the deposition mask is removed by sonicating the entire substrate in a solvent. An array of triangularly shaped nanoparticles with P_{6mm} symmetry remains on the substrate. The 3D shape of the individual nanoparticles is approximately that of a truncated tetrahedron.[74] Through manipulation of the parameters D and d_m, the in-plane width and out-of-plane height of the nanoparticles can be independently tuned with a few nanometer precision. Additionally, nanoparticle shape is controlled by the precision of the deposition mask, or alternatively, by postdeposition processing steps such as thermal annealing.

Recently, we demonstrated that the peak extinction, λ_{max}, for NSL-fabricated Ag nanoparticles was highly dependent upon the refractive index of the surrounding medium, $n_{external}$.[73] In these studies, nanoparticles with in-plane widths of 100 nm and out-of-plane heights of 50 nm exhibited LSPR shifts of 200 nm per refractive index unit (RIU). These experiments suggested that Ag nanoparticles could be used in sensor applications much like the widely available biosensors that operate using propagating surface plasmon polaritons (SPP) generated from smooth metal films.[34] SAMs are extensively used in many sensor technologies since they can functionalize a surface for specific analyte capture and protect biological surfaces from denaturing upon exposure to metal surfaces.[33−35] Thus, the optical characterization of SAM-modified nanoparticles is a fundamental step in assessing the usefulness of these systems in sensing applications.

Several inherent features of NSL make it an excellent technique to study chemically modified nanoparticles. With NSL, the nanoparticles are confined to a surface at a fixed interparticle spacing determined by the size of the nanosphere mask. Unlike colloids, NSL fabricated nanoparticles do not rely on repulsive forces from surface anions to keep them separated or suspended in solution. Consequently, flocculation caused by displacement of surface charges does not occur. Unlike the Au thiol capped nanoparticles by Brust et al.,[38] NSL nanoparticles are readily modified after nanoparticle formation. Therefore, detailed studies of the optical properties of the nanoparticles before and after chemical modification with SAMs are possible.

In this paper, we present a detailed study of the LSPR of Ag nanoparticles fabricated by NSL and chemically modified with alkanethiols, $CH_3(CH_2)_xSH$ of chain length $x = 3-15$. As part of this investigation, we will first demonstrate that the nanoparticles undergo structural changes when exposed to various solvents which significantly affect the LSPR. Optical contributions of the SAM will be assessed by measuring the macroscale UV−vis extinction spectrum before and after thiol modification. We will show that λ_{max} shifts to the red 3 nm for every carbon atom in the alkanethiol chain. Additionally, we will demonstrate that spectral shifts as large as 40 nm are caused by the adsorption of only 60 000 molecules per nanoparticle, which corresponds to 100 zmol of adsorbate. A reasonable extrapolation suggests that optimized experiments on single nanoparticles may have a detection limit of ~2.5 zmol. Results will also be presented that demonstrate that the sensitivity to bulk liquid is only diminished by 20% when the nanoparticles are modified with the longest alkanethiol we studied here, C_{15}. Mie theory calculations on Ag core−shell nanoparticles with dielectric shells that simulate alkanethiol SAMs in thickness and dielectric constant will be presented. These calculations can be used to predict trends in the experimental extinction data of SAM-modified nanoparticles. We will also demonstrate that functionalized Ag nanoparticles can detect changes in refractive index induced by analyte binding events. Specifically, we detected LSPR shifts induced by the electrostatic binding of

(65) Barnickel, P.; Wokaun, A. *Mol. Phys.* **1989**, *67*, 1355−1372.
(66) Oldenburg, S. J.; Averitt, R. D.; Westcott, S. L.; Halas, N. J. *Chem. Phys. Lett.* **1998**, *288*, 243−247.
(67) Weisbecker, C. S.; Merritt, M. V.; Whitesides, G. M. *Langmuir* **1996**, *12*, 3763−3772.
(68) Sastry, M.; Lala, N.; Patil, V.; Chavan, S. P.; Chittiboyina, A. G. *Langmuir* **1998**, *14*, 4138−4142.
(69) Sastry, M.; Mayya, K. S.; Patil, V.; Paranjape, D. V.; Hegde, S. G. *J. Phys. Chem. B* **1997**, *101*, 4954−4958.
(70) Mayya, K. S.; Sastry, M. *Langmuir* **1998**, *14*, 6344−5346.
(71) Hulteen, J. C.; Van Duyne, R. P. *J. Vac. Sci. Technol. A* **1995**, *13*, 1553−1558.
(72) Hulteen, J. C.; Treichel, D. A.; Smith, M. T.; Duval, M. L.; Jensen, T. R.; Van Duyne, R. P. *J. Phys. Chem. B* **1999**, 3854−3863.
(73) Jensen, T. R.; Duval, M. L.; Kelly, L.; Lazarides, A.; Schatz, G. C.; Van Duyne, R. P. *J. Phys. Chem. B* **1999**, 9846−9853.
(74) Jensen, T. R.; Schatz, G. C.; Van Duyne, R. P. *J. Phys. Chem. B* **1999**, 2394−2401.

the cationic polypeptide, poly-L-lysine (PL) to Ag nanoparticles modified with deprotonated carboxylate groups from 11-mercaptoundecanoic acid. Furthermore, we will show that these nanosensors behave reversibly and exhibit no detectable nonspecific binding.

The remainder of this paper is organized as follows. In section II, we discuss the details of the techniques and methods used here to fabricate, characterize, and modify the Ag nanoparticles used here. A description of the theoretical methods will also be given. In section III, we present and discuss experimental data and compare the results to Mie theory core−shell calculations. In section IV, our results and conclusions will be summarized.

II. Experiment and Methods

Materials. 1-Hexadecanethiol (1-HDT), 1-dodecanethiol (1-DDT), 1-decanethiol (1-DT), 1-octanethiol (1-OT), 1-hexanethiol (1-HT), 1-butanethiol (1-BT), and 11-mercaptoundecanoic acid (11-MUA) were purchased from Aldrich (Milwaukee, WI) and used without further purification. 1-Tetradecanethiol (1-TDT) was purchased from Fluka and also used without further purification. Poly-L-lysine (PL), MΩ = 41 000, and phosphate buffered saline (PBS) were obtained from Sigma (St. Louis, MO). Absolute ethanol was acquired from Pharmco. Ag (99.99%, 0.50 mm diameter) was purchased from D. F. Goldsmith (Evanston, IL). Borosilicate glass substrates were Fisherbrand No. 2 18 mm circle cover slips from Fisher Scientific. Tungsten vapor deposition boats were acquired from R. D. Mathis (Long Beach, CA). Polystyrene nanospheres from Interfacial Dynamics Corporation (Portland, OR) with diameters of 400 ± 7 nm were received as a suspension in water and were used without further treatment. For all steps of substrate and sample preparation, water purified with cartridges from Millipore (Marlborough, MA) to a resistivity of 18 MΩ was used.

Substrate Preparation. Glass substrates were cleaned by immersion in piranha solution (3:1 concentrated H_2SO_4:30% H_2O_2) at 80 °C for 1 h. After cooling, the substrates were rinsed repeatedly with water and then sonicated for 60 min in 5:1:1 H_2O:NH_4OH:30% H_2O_2. Following sonication, the substrates were repeatedly rinsed with copious amounts of water. Substrates were either used immediately or stored in water for no longer than one week.

Preparation of Periodic Particle Arrays. Nanosphere lithography was used to fabricate arrays of nanoparticles on glass substrates.[71,72] For all the experiments presented here, the single layer colloidal crystal nanosphere deposition mask was prepared by drop coating 2−5 μL of the nanosphere suspension onto the substrate where the nanospheres were allowed to self-assemble into a hexagonally closed-packed monolayer as the water evaporated. Once the masks were formed, the samples were mounted into the chamber of a Consolidated Vacuum Corporation vapor deposition chamber. A Leybold Inficon XTM/2 deposition quartz crystal microbalance (East Syracuse, NY) was used to measure the thickness of the Ag film deposited over the nanosphere masks. For all the samples used here, the Ag films were grown to a thickness of 50 nm. After the Ag deposition, the nanosphere mask was removed by sonicating the entire substrate in ethanol for at least 2 min.

Ultraviolet−Visible Extinction Spectroscopy. Macroscopic UV−vis extinction measurements were performed on an Ocean Optics (Dunedin, FL) SD2000 fiber optically coupled spectrometer with a CCD detector. All spectra shown here were macroscopic measurements performed in standard transmission geometry with unpolarized light impinging upon the surface at a normal angle of incidence. The probe beam area was approximately 5 mm^2. The spectra shown here are the average of 25 individual 100 ms integrations.

Nanoparticle Modification. A custom built flow cell, shown in Figure 1, was used to control the external environment of the nanoparticle array throughout the entire experiment. Prior to SAM modification, various solvents (methanol, acetone, ethanol, or methylene chloride) followed by dry N_2 gas were cycled through the flow cell until the UV−vis spectrum of the nanoparticle array repeatedly returned to the same spectral location in N_2. Once the spectrum stabilized, a SAM solution of a given alkanethiol, approximately 1 mM in ethanol, was introduced into the cell. The valves on the needle input and output ports were then closed to allow the SAM solution to incubate with the nanoparticle array for 10−24 h. After incubation, the SAM solution was removed and copious amounts of ethanol were flushed through the cell to rinse the nanoparticles of any unbound thiol. The nanoparticles were then dried by flowing N_2 through the cell.

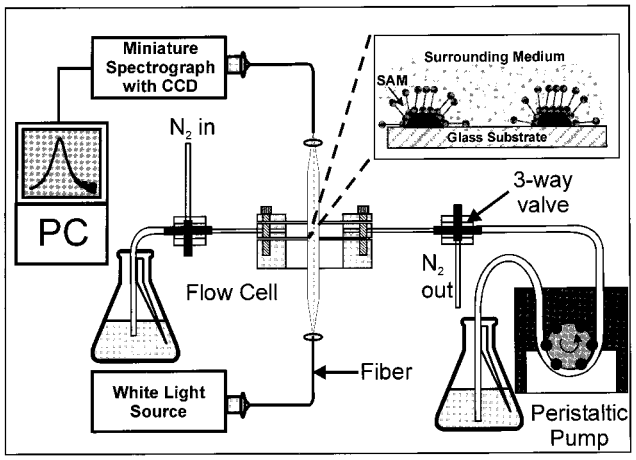

Figure 1. Instrumental diagram of the LSPR sensor experiment. The inset shows a schematic diagram of the SAM-modified nanoparticles in a surrounding medium, either solvent, buffer, or gas.

Atomic Force Microscopy (AFM) Measurements. AFM images were collected on a Digital Instruments Nanoscope III microscope operating in tapping mode. Etched Si nanoprobe tips (TESP, Digital Instruments, Santa Barbara, CA) were used. These tips had resonance frequencies between 280 and 320 kHz and are conical in shape with a cone angle of 20° and an effective radius of curvature at the tip of 10 nm. All images shown here are raw, unfiltered data that were collected under ambient laboratory conditions.

Theoretical Calculations. The theory used here is an extension of Mie theory, which is the solution of Maxwell's equations for an isotropic sphere. Here, surrounded by an infinite external medium, there are two concentric regions of material: a spherical core of silver and a uniform coating of dielectric material of specified thickness. This is known as a concentric or layered sphere problem,[75] and expressions for the extinction cross-sections have been programmed in a FORTRAN code (BHCOAT)[76] that is publicly available.

Required input for BHCOAT are dielectric constants for each material (core, shell, and external media) and size information for each region. All calculations were performed with a 30 nm radius Ag core. This radius makes the particle have the same volume as the NSL-fabricated nanoparticle. The wavelength-dependent bulk dielectric constants from Palik[77] were used. For the variable thickness SAM coating, the value of the refractive index for neat alkanethiol as reported by Aldrich, $n_{SAM} = 1.42$, was used. Extinction efficiencies produced by BHCOAT were corrected by the cross-sectional area of the Ag core to give the extinction efficiency referenced to the Ag particle only. This choice makes it easier to visualize the effect of the SAM on the absolute extinction, as well as on the LSPR peak location.

III. Results and Discussion

Solvent-Induced Changes in Ag Nanoparticle Structure. Although the major objective of this paper was to optically characterize Ag nanoparticles modified with SAMs, considerable effort was made to understand the structural changes that occur when unmodified Ag nanoparticles are exposed to organic solvents and/or aqueous electrolyte solutions. A major thrust behind the study of nanoparticle optics is the creation of new materials for sensor and spectroscopy applications. These

(75) Aden, A. L.; Kerker, M. *J. Appl. Phys.* **1951**, *22*, 1242−1246.
(76) Bohren, C. F.; Huffman, D. R. *Absorption and Scattering of Light by Small Particles*; Wiley-Interscience: New York, 1983.
(77) Palik, E. D. *Handbook of Optical Constants of Solids*; Academic Press: New York, 1985.

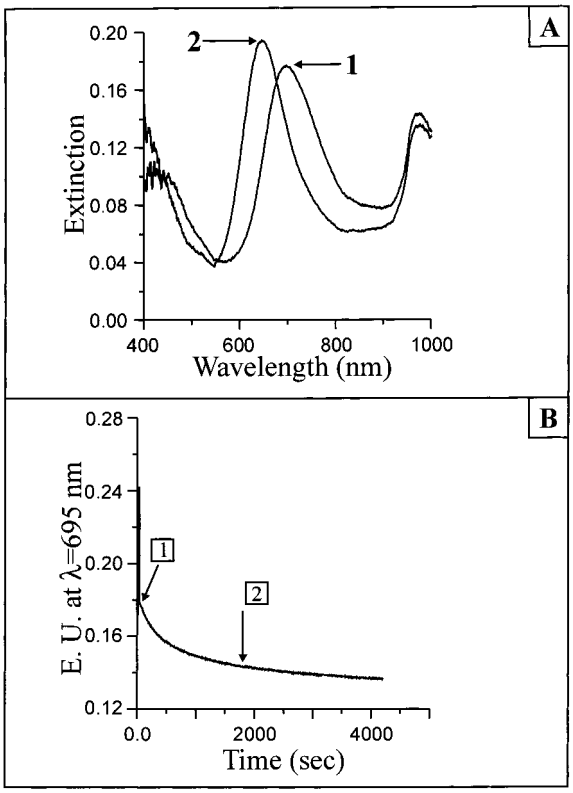

Figure 2. (A) Extinction spectrum of a Ag nanoparticle array (D = 400 nm, d_m = 50 mm) on a glass substrate in H_2O: (1) initially (time $\approx$ 0 s), λ_{max} = 695 nm, and (2) 30 min later, λ_{max} = 647 nm (B). The extinction intensity at λ = 695 nm as a function of time. The spike in intensity observed at t = 0 is due to scattering of the probe light caused by the rapid turbulence of the water as it is initially pushed through the flow cell.

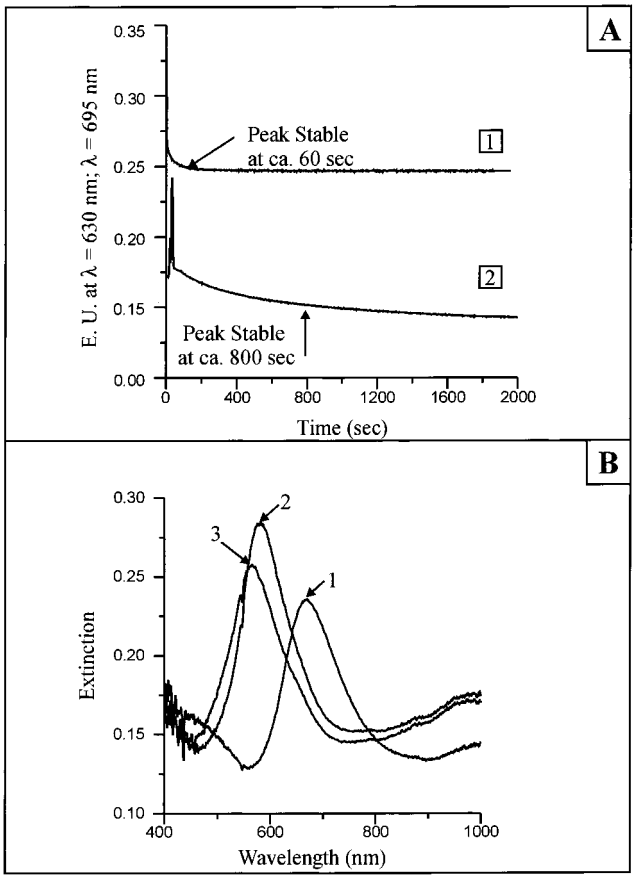

Figure 3. (A) Comparison of extinction time curves for subsequent exposures to solvent: (1) the extinction intensity at λ = 630 nm as a function of time for the nanoparticles second exposure to a solvent, methanol and (2) the extinction intensity at λ = 695 nm as a function of time for the nanoparticles first exposure to water. Plot (2) presents the same data shown in Figure 2B. (B) Extinction spectrum for the same Ag nanoparticle array recorded in a N_2 environment: (1) prior to any solvent exposure, λ_{max} = 668 nm; (2) after the first cycle of H_2O, λ_{max} = 582 nm; and (3) after the second cycle of methanol, λ_{max} = 566 nm.

applications typically involve mass transport of the adsorbate or analyte to the surface through a solution environment. In a similar sense, an intrinsic feature of the SAM formation process is exposure of the metal surface to the solvent in which the alkanethiol molecules are dissolved. Thus, the stability of Ag nanoparticles in liquid solution environments is an important issue. To this end, we will first present results that address solvent-induced structural and consequently optical changes in Ag nanoparticles prior to surface modification with SAMs.

Previously, Roark and Rowlen[78] demonstrated that Ag island films undergo structural changes, namely height increases, when exposed to certain solvents such as methanol and acetone. As a result of the height increase, a blue shift in the optical extinction maximum, λ_{max}, was also observed. We have shown that the λ_{max} of the LSPR of NSL-fabricated Ag nanoparticles is extremely sensitive to the height of the individual nanoparticles.[79] In Figure 2A, we show the LSPR spectra of Ag nanoparticles in water at two different time increments during an incubation process. The spectrum denoted in Figure 2A-1 was collected when water was first introduced into the cell at time t $\approx$ 0 s. Thirty minutes later, the spectrum labeled Figure 2A-2 was recorded. During the 30 min exposure to water, the LSPR shifts to the blue by approximately 48 nm from 695 to 647 nm. The extinction intensity at λ = 695 nm, with λ_{max} at t $\approx$ 0, was monitored as a function of time. Figure 2B displays the resulting time evolution of the LSPR extinction. Here, it is apparent that the peak position seems relatively stable at approximately 30 min. After the water cycle, the nanoparticles were dried using N_2 and subsequently exposed to a second solvent, methanol. Again, the λ_{max} initially observed at $t \approx 0$ for the methanol cycle was monitored as a function of time. The resulting time curve is shown in Figure 3A where the time plot from Figure 2B is overlaid to serve as a comparison. Here, it is evident that the LSPR peak location stabilizes much more quickly for the second solvent cycle. Figure 3B shows the extinction spectra for this same array recorded in N_2 at three different intervals: (1) prior to any solvent exposure, (2) after the first cycle of water, and (3) after the second cycle of methanol. This figure demonstrates the dramatic effect on the LSPR induced by solvent exposure. For this sample, λ_{max} shifted to the blue by approximately 100 nm after two lengthy solvent cycles.

Panels A and B in Figure 4 display AFM images of a Ag nanoparticle array recorded before and after exposure to water, respectively. At first, the two images appear to be almost identical, but after careful inspection subtle differences are apparent. Exposure to water seems to have at least two major effects: (1) the average height of the nanoparticles increased from 47.3 $\pm$ 1 to 51.3 $\pm$ 2 nm and (2) the tips of the nanoparticles appear to be more rounded. In another study, we demonstrated that for NSL-fabricated nanoparticles of this approximate size, a 1 nm increase in particle height produces a

(78) Roark, S. E.; Rowlen, K. L. *Anal. Chem.* **1994**, *66*, 261−270.
(79) Jensen, T. R.; Duval Malinsky, M.; Haynes, C. L.; Van Duyne, R. P. *J. Phys. Chem. B* **2000**, *104*, 10549−10556.

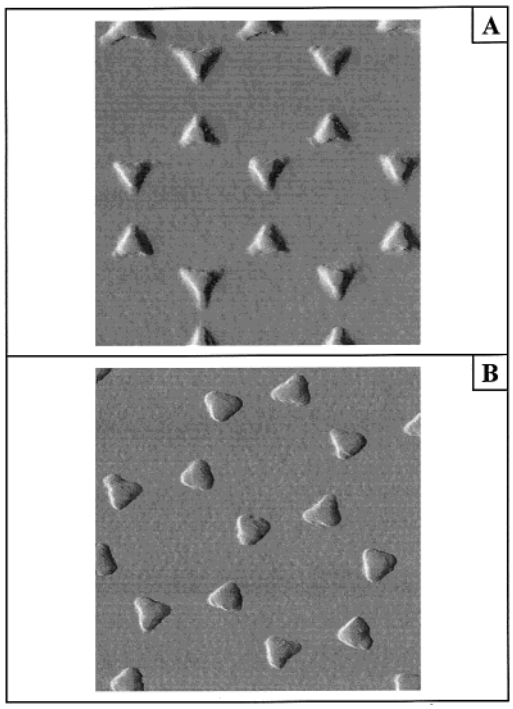

Figure 4. Tapping mode AFM images of the Ag nanoparticle array (D = 400 nm, d_m = 50 nm) on glass substrates: (A) 1 μm × 1 μm image of nanoparticles not exposed to any solvent after nanosphere mask removal (the average particle height was measured to be 47.3 ± 1 nm) and (B) 1 μm × 1 μm image of nanoparticles after incubation in H_2O for 24 h (the average particle height was measured to be 51.3 ± 2 nm).

5 nm spectral shift to the blue.[79] If increase in particle height was the sole factor responsible for the 100 nm shift observed here, it would indicate that the particles would have had to increase in height by 20 nm, roughly 40% of the initial height. The AFM measurements only recorded a height increase of 4 nm. Therefore, we can attribute only about 20 nm of the total 100 nm shift to changes in height. This same study also showed that changes in nanoparticle shape can have an even more dramatic effect on the LSPR λ_{max}. By using a thermal annealing procedure, the in-plane cross-sectional shape of the nanoparticles was changed from triangular to ellipsoidal.[79] This morphology change resulted in a blue shift of λ_{max} of over 200 nm. Although the nanoparticles shown here still retain most of their triangular shape after exposure to water, evidence of the tips rounding after solvent treatment is apparent when comparing AFM images in Figure 4A,B. Therefore, we believe that the other 80 nm of blue shift is the result of slight changes in shape.

Over the course of these experiments, values of λ_{max} were recorded in N_2 environments for several solvent-treated Ag nanoparticle arrays on glass substrates. In Figure 5, a histogram displays the range of λ_{max} values recorded. It should be noted that for all the measurements shown in Figure 5 that cycles of solvent and N_2 were repeated until the LSPR peak in N_2 no longer blue-shifted after exposure to solvent (primarily methanol, acetone, and ethanol). The average λ_{max} was calculated to be 560 ± 12 nm. If one considers that a 1 nm change in height roughly corresponds to a 3−5 nm change in λ_{max}, then the observed λ_{max} standard deviation of 12 nm approximately correlates to the measured standard deviation in nanoparticle height of 2 nm.

Mechanism of Solvent-Induced Changes in Ag Nanoparticle Structure. Here we consider the origin of the Ag nanoparticle structural changes induced by exposure to water

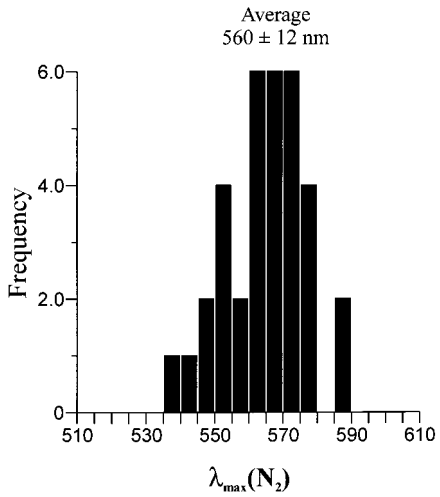

Figure 5. Histogram of stabilized λ_{max} values in N_2 after exposure to solvent. All measurements were recorded for Ag nanoparticle arrays fabricated with D = 400 nm and d_m = 50 nm. The average value of λ_{max} was calculated to be 560 ± 12 nm.

(Figure 4A,B), which results in an increase of their average height from 47.3 ± 1 to 51.3 ± 2 nm and a "rounding" of their tips. At least three mechanisms require consideration: (1) surface melting,[72] (2) surface oxidation of Ag nanoparticles, and (3) nanoparticle−substrate interaction.

The structural changes observed in Figure 4 involve nanoparticles with a constant in-plane size (~100 nm) but a change in the external environment from laboratory ambient (air) to water. Since the onset of size-dependent surface melting occurs at ~100 nm, it is more likely that surface oxidation or nanoparticle−substrate interactions rather than surface melting are the dominant mechanisms.

There is no question that Ag nanoparticles fabricated by NSL and handled in the laboratory ambient acquire a surface oxide layer upon removal from the vacuum deposition chamber. Direct characterization of the surface oxide by X-ray photoelectron spectroscopy (XPS) or electrochemical studies is not possible for the Ag nanoparticle on glass system used for these nanosensor experiments since the substrate is not electrically conductive. Nonetheless, some comment on the thickness of the putative surface oxide layer can be made. In recent combined theory and experimental studies, we have demonstrated that most features of the LSPR spectrum of Ag nanoparticles on mica and glass substrates can be accurately captured without specific inclusion of an oxide layer.[74,80] Thus we conclude that surface oxidation contributes at most a thin (viz., <1 nm) shell of material. The effect of surface oxide formation on the shape and LSPR spectrum of small (~20 nm) spherical Ag nanoparticles supported on silica sol−gels has been previously reported.[81] In that study, it was found that oxide formation resulted in a red-shift of the LSPR and a reduction of nanoparticle height accompanying a spherical to oblate spheroid shape change. We observe the opposite in our experiments. Thus we conclude that, while surface oxidation definitely does occur, it is not the dominant factor in determining the nanoparticle shape changes (Figure 4) and LSPR shifts (Figure 5) reported here.

The role of the nanoparticle−substrate interactions is conveniently examined within a surface thermodynamic framework and requires consideration of the relative values of the surface

(80) Kelly, L.; Jensen, T. R.; Lazarides, A.; Schatz, G. C. *Modeling Nanoparticle Optical Properties*; Feldheim, D. L., Foss, C. A., Jr., Eds.; Marcel-Dekker: New York, 2000, in press.

(81) Yanase, A.; Komiyama, H. *Surf. Sci.* **1992**, *264*, 147−156.

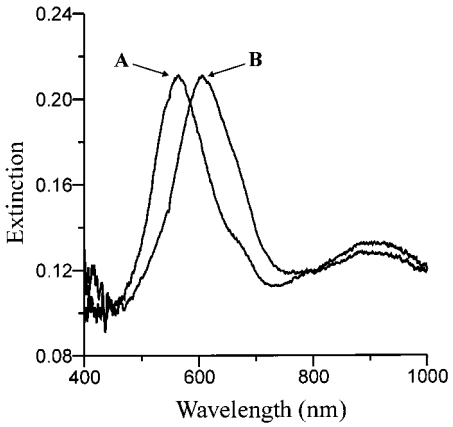

Figure 6. UV−vis extinction spectra of Ag nanoparticle arrays on glass in a N_2 environment: (A) nanoparticles before chemical modification, $\lambda_{max} = 564$ nm, and (B) nanoparticles after modification with 1-HDT, C_{15}, $\lambda_{max} = 604$ nm.

tensions (viz., free energy per unit area) γ_0, γ_i, and γ_s corresponding to the Ag/ambient (or water), Ag/substrate, and substrate/ambient (or water) interfaces, respectively.[82] Under circumstances where $\gamma_0 + \gamma_i < \gamma_s$, Ag would better wet the substrate and one expects an increase in in-plane nanoparticle size accompanied by a decrease in nanoparticle height. Conversely, if $\gamma_0 + \gamma_i > \gamma_s$, Ag would better dewet the substrate adopting a more compact shape with a decrease in in-plane nanoparticle size and an increase in nanoparticle height. Thus, the issue of water (solvent)-induced nanoparticle reconstruction reduces to the effect of water (solvent) exposure on the relative values of γ_0, γ_i, and γ_s. Assuming that the Ag nanoparticle strongly adheres to the substrate preventing water (solvent) from penetrating the Ag/substrate interface, γ_i probably remains unchanged. In contrast, both γ_0 and γ_s will be decreased by the presence of adsorbed water (solvent) at the Ag/ambient and substrate/ambient interfaces.[82−84] Since the glass substrates used here are highly hydrophillic, it is plausible that γ_s is decreased more strongly than γ_0. Thus, $\gamma_0 + \gamma_i > \gamma_s$ will remain true leading to a decrease in in-plane nanoparticle size (viz., tip "rounding" and retraction) and an increase in nanoparticle height as is observed experimentally. Thus, we conclude that the dominant factor in water (solvent)-induced nanoparticle reconstruction is likely to be the strong decrease in surface tension at the hydrophillic glass/water interface.

SAM-Modified Ag Nanoparticles. Before modification with alkanethiol SAMs, the external environment of all the Ag nanoparticle arrays was cycled between a solvent and N_2 as described above. Since exposure to solvent is required for SAM formation, our intention was to force any solvent-induced structural changes to occur before modification with the alkanethiol. This would allow us to unambiguously attribute LSPR spectral shifts to the presence of the SAM and not to particle restructuring that occurred during SAM formation. Figure 6 shows the UV−vis extinction spectrum of a Ag nanoparticle array in a controlled N_2 environment ($n_{external} = 1.0$) before and after modification with 1-hexadecanethiol, 1-HDT. After modification with the SAM, the LSPR λ_{max} shifts to the red 40 nm from 564 to 604 nm. The red shift in the extinction spectrum is to be expected because the external dielectric constant, ϵ (where $\epsilon = n_{external}^2$), of the Ag nanoparticles increased from $\epsilon = 1.0$ for N_2 to $\epsilon \approx 2.10$ for the SAM. However, such a large shift in the LSPR caused by one monolayer of adsorbate was not anticipated based on prior experiments[85] or theoretical predictions.[73] The magnitude of the shift is quite remarkable when one considers the small number of 1-HDT molecules that are involved.

Table 1. Extinction Data for Ag Nanoparticle Arrays ($D = 400$ nm, $d_m = 50$ nm) on Glass Modified with Alkanethiol SAMs of Various Chain Lengths

SAM $CH_3(CH_2)_xSH$	C_x	λ_{max} (nm) in N_2 after SAM modification	λ_{max} (nm) in N_2 before SAM modification	$\Delta\lambda_{max}$ (nm)
1-HDT	C_{15}	604	564	40
1-TDT	C_{13}	620	585	35
1-DDT	C_{11}	577	550	27
1-DT	C_9	585	566	19
1-OT	C_7	577	566	11
1-HT	C_5	581	573	8
1-BT	C_3	558	556	2

In previous studies, we have demonstrated two important features of NSL-fabricated Ag nanoparticles: (1) macroextinction spectra with probe beam areas of 4 mm^2 or greater are equivalent to spatially resolved microextinction spectra with probe beam areas of 12 μm^2,[73] and (2) Ag nanoparticles fabricated with $D = 400$ nm spheres are spaced sufficiently far apart that they do not electromagnetically couple.[74] The combination of these two results proves that the extinction spectrum from a single nanoparticle is equivalent to that of the array. Thus, for modification with 1-HDT, the 40 nm shift measured in the macroscopic experiments presented here would also be observed in a NSOM experiment interrogating a single nanoparticle. By using simple geometry and the approximation that the 3D nanoparticle shape is that of a truncated tetrahedron,[74] the surface area of the Ag nanoparticle accessible for SAM modification in these experiments is calculated to be 1.4×10^{-10} cm^2. Given that the packing density of 1-HDT is 4.4×10^{14} molecules cm^{-2},[86] a maximum of 6×10^4 1-HDT molecules can be adsorbed on each nanoparticle. Therefore, $\Delta\lambda_{max} = 40$ nm corresponds to only 100 zmol of adsorbate. Assuming that a 1 nm LSPR shift can readily be measured on a single nanoparticle with NSOM, we estimate a detection limit on the order of 1500 molecules per nanoparticle or 2.5 zmol per nanoparticle. Alternatively, the detection limit is equivalent to 2−3% of a monolayer of 1-HDT on a single nanoparticle.

The dependence of the LSPR shift, $\Delta\lambda_{max}$, on alkanethiol chain length, x, was also studied in detail. Table 1 lists values of λ_{max} for Ag nanoparticle arrays in a N_2 environment both before and after modification with a given alkanethiol. The dependence of the LSPR shift, $\Delta\lambda_{max}$, on alkanethiol chain length, x, is illustrated in Figure 7. The slope and intercept of this plot yield important new information concerning the effect of the local dielectric environment (i.e., product of dielectric constant and thickness) of the SAM shell and the Ag−S chemisorption on the LSPR. First, it is evident that the LSPR shifts to the red 3 nm for every carbon atom in the alkanethiol chain. Since the refractive index of all the neat alkanethiols used here is roughly constant, we attribute the linear dependence on the chain length solely to an increase in the thickness of the SAM shell. Second, the linear fit of the data produces a negative

(82) Zangwill, A. *Physics at Surfaces*; Cambridge University Press: Cambridge, 1988.
(83) Israelachvili, J. *Intermolecular and Surface Forces*, 2nd ed.; Academic Press: San Diego, 1992.
(84) Somorjai, G. A. *Introduction to Surface Chemistry and Catalysis*; John Wiley & Sons: New York, 1994.
(85) Templeton, A. C.; Pietron, J. J.; Murray, R. W.; Mulvaney, P. *J. Phys. Chem. B* **2000**, *104*.
(86) Li, J.; Liang, K. S.; Camillone, N., III; Leung, T. Y. B.; Scoles, G. *J. Chem. Phys.* **1995**, *102*, 5012−5028.

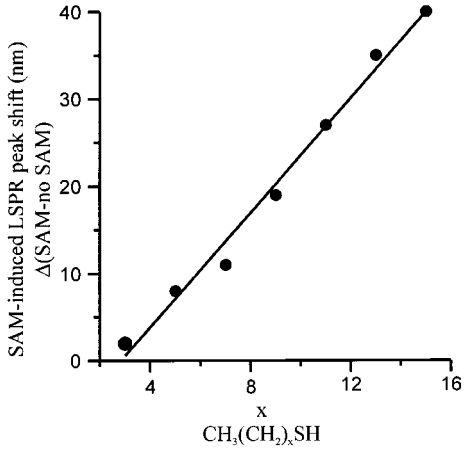

Figure 7. Alkanethiol chain length dependence on the LSPR spectral peak shift. All extinction measurements were collected in a N_2 environment ($n_{external} = 1.0$). Linear regression was used to fit the data to a line described by the following equation: $y = 3.3(x) - 9.3$.

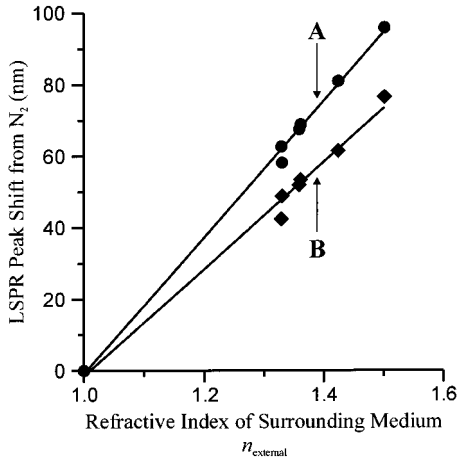

Figure 8. Ag nanoparticle sensitivity to bulk solvent. Spectral peak shifts were calculated by subtracting the measured extinction maximum, λ_{max}, for the nanoparticles in solvents of $n_{external}$ ranging from 1.33 (methanol) to 1.51 (benzene) from that of a N_2 environment ($n_{external} = 1.0$). Plots display representative measurements from several experiments. (A) Unmodified nanoparticles. The slope of the linear fit shows that the LSPR spectral sensitivity to $n_{external}$ is 191 nm per refractive index unit (RIU). (B) Nanoparticles modified with 1-HDT. The slope of the linear fit is reduced by 20% to 150 nm RIU^{-1}.

y-intercept. This feature can be explained by the charge-transfer interaction resulting from the formation of the Ag−S chemisorption bond. The electron-donating S atom alters the surface electronic structure of the nanoparticle (increasing the electron density) resulting in a blue shift of the LSPR.[25] This concept has been previously used to explain the blue shift in the LSPR observed upon chemisorption of SH^- on colloidal Ag.[87] Results similar to those shown in Figure 7 were previously reported in connection with ellipsometric measurements of the thickness of alkanethiols adsorbed on gold films.[88] In this investigation, a linear dependence of the measured alkanethiol film thickness on chain length was observed. This was interpreted as a structural consequence of these systems being dense, well-packed monolayers. Therefore, we believe that the linear chain length dependence shown in Figure 7 is evidence of the existence of dense, well-packed alkanethiol SAMs on the large Ag nanoparticles described here. The ellipsometric data also produced a negative intercept similar to that reported here. However, the authors attributed this feature to the removal of surface contamination upon formation of the monolayer.

Sensitivity to Bulk Liquid Interface. One goal of studying chemically modified nanoparticles is their use in chemical and biological sensor applications. For *in situ* applications, the ability to measure changes in refractive index that occur at a SAM/bulk liquid interface is critical. In Figure 8, we show the response of $\Delta\lambda_{max}$ to changes in the bulk dielectric produced by exposing the unmodified and SAM-modified Ag nanoparticles to a sequence of solvents (methanol, acetone, ethanol, methylene chloride, and benzene). For both cases, the sensitivity to external environment is linearly dependent on the refractive index of the solvent, $n_{external}$. From the slopes of the linear fits, we extract sensitivity factors, $\Delta\lambda_{max}/\Delta n_{external}$, of 191 and 150 nm RIU^{-1} for the unmodified and 1-HDT-modified Ag nanoparticles, respectively. Thus, the presence of the 1-HDT monolayer diminishes the sensitivity to $n_{external}$ by approximately 20%. This observation is not surprising when considering the spatial distribution of the electromagnetic fields surrounding the Ag nanoparticles. When the LSPR is excited, the strength of the generated electromagnetic fields decays over the length scale of ~50 nm.[89] Thus, the strongest sensing capabilities are in the near surface region of the nanoparticle. The dense SAM shell that surrounds the nanoparticle acts as a barrier preventing solvent molecules from penetrating to the surface. Hence, the SAM barrier moves the sensing region farther away from the surface of the nanoparticle where the electromagnetic fields are weaker. Although the sensitivity is diminished by 20% with the SAM, bulk solvent induced shifts are still easily detected. This indicates that the electromagnetic fields extend far enough away from the nanoparticle to sense refractive index changes occurring at the SAM/bulk interface.

Mie Theory Core Shell Calculations. In previous work, we have used the discrete dipole approximation (DDA) to model the optical properties of NSL fabricated nanoparticles.[73,74,89] The appeal of DDA lies in its ability to calculate the optical properties that match experimental results with a high degree of accuracy without employing any adjustable parameters. Although DDA is an extremely powerful computational method, the calculations become cumbersome when using multicomponent systems to account for an inhomogeneous nanoparticle environment (substrate, dielectric overlayers, and the bulk medium). Mie theory is a much simpler method to calculate the optical properties of nanoparticles of spherical shape and it can also be used to provide semiquantitative insight about nonspherical nanoparticles. Here, we use Mie theory to model the contribution of SAM dielectric overlayers on Ag nanospheres.

Figure 9 displays the extinction efficiencies for a Ag nanosphere with radius = 30 nm surrounded by dielectric shells of $n = 1.42$ of increasing thickness, t, in a vacuum, $n_{external} = 1.0$. As the shell thickness increases, the extinction shifts to the red and becomes stronger. Given that a 1-HDT monolayer is approximately 2 nm thick,[88,90,91] Mie theory predicts that encapsulation of a Ag nanosphere with a 1-HDT monolayer would shift the LSPR approximately 11 nm. This shift is only approximately 25% of what was measured experimentally for oblate NSL-fabricated nanoparticles. A recent study by the

(87) Linnert, T.; Mulvaney, P.; Henglein, A. *J. Phys. Chem.* **1993**, *97*, 679−682.
(88) Bain, C. D.; Troughton, E. B.; Tao, Y.-T.; Evall, J.; Whitesides, G. M.; Nuzzo, R. G. *J. Am. Chem. Soc.* **1989**, *111*, 321−335.
(89) Jensen, T. R.; Kelly, L.; Lazarides, A.; Schatz, G. C. *J. Clust. Sci.* **1999**, *10*, 295−317.
(90) Peterlinz, K. A.; Georgiadis, R. *Langmuir* **1996**, *12*, 4731−4740.
(91) Jung, L. S.; Campbell, C. T.; Chinowsky, T. M.; Mar, M. N.; Yee, S. S. *Langmuir* **1998**, *14*, 5636−5648.

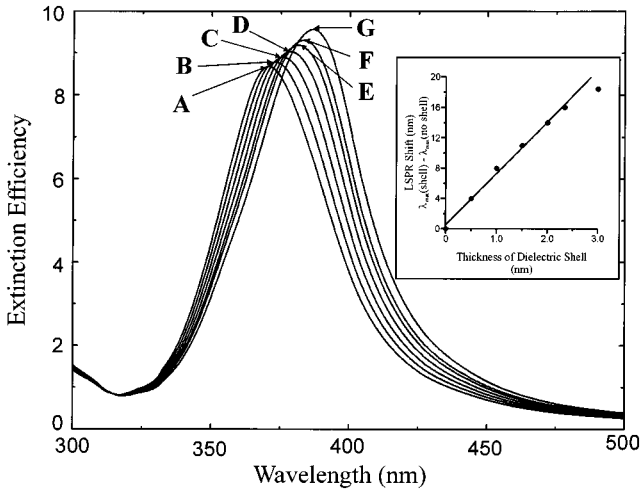

Figure 9. Extinction spectra of Ag nanospheres (radius = 30 nm) with dielectric shells ($n = 1.42$) of varying thickness, t, calculated using Mie theory. $n_{external} = 1.0$: (A) $t = 0$ nm, $\lambda_{max} = 370.7$ nm; (B) $t = 0.5$ nm, $\lambda_{max} = 373.1$ nm; (C) $t = 1.0$ nm, $\lambda_{max} = 375.8$ nm; (D) $t = 1.5$ nm, $\lambda_{max} = 378.3$ nm; (E) $t = 2.0$ nm, $\lambda_{max} = 381.3$ nm; (F) $t = 2.34$ nm, $\lambda_{max} = 383$ nm; and (G) $t = 3.0$ nm, $\lambda_{max} = 386.7$ nm. The inset illustrates the dielectric shell thickness dependence upon the LSPR spectral shift. When the $t = 3.0$ nm point was excluded, the data were fit to a line with the equation $y = 6.2(x) + 10$.

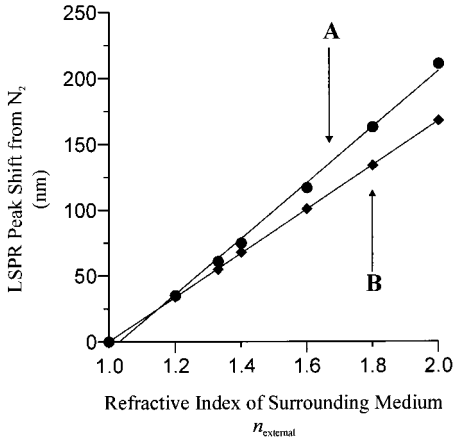

Figure 10. Sensitivity to bulk external solvent for Ag nanospheres (radius = 30 nm) with and without a dielectric shell calculated with use of Mie theory. Spectral peak shifts were obtained by subtracting λ_{max} for the Ag nanospheres in $n_{external}$ ranging from 1.33 (methanol) to 1.51 (benzene) from that of a N_2 environment ($n_{external} = 1.0$). (A) No dielectric shell: The slope of the linear fit shows that the LSPR spectral sensitivity to $n_{external}$ is 212 nm RIU^{-1}. (B) Ag nanosphere with a 2.0 nm thick dielectric shell of $n = 1.42$: The slope of the linear fit is reduced by 20% to 168 nm RIU^{-1}.

Murray and Mulvany groups[85] presented Mie theory calculations on Au cores with SAM shells of varying thickness. The calculations in this study found that the LSPR of 5.2 nm diameter Au nanoparticles in water shifted to the red by 7 nm when the thickness of the SAM shell was increased from 0 to 2 nm. Additionally, this same study presented Mie theory calculations which demonstrated that the LSPR of Au nanoparticles capped with a 1 nm alkanethiol shell shifts approximately 8 nm when $n_{external}$ is changed from 1.33 to 1.55. This calculated shift agreed with what was observed experimentally for 5.2 nm diameter Au colloids capped with 1-dodecanethiol. These findings indicate that differences in nanoparticle shape probably account for much of the discrepancy seen between the Mie theory calculations presented here and the experimental results. Recently, we demonstrated that nanoparticles whose cross-sectional in-plane shape is more ellipsoidal than triangular are less sensitive to changes to $n_{external}$.[73] Thus, it is not surprising that the completely spherical nanoparticles used in the Mie theory calculations are not as sensitive as oblate nanoparticles with 2:1 aspect ratios (width:height). Also, Mie theory only accounts for the dielectric properties of the simulated SAM shell. In the experimental work, the SAM shell is chemisorbed through electron donation from the sulfur atom into the Ag nanoparticle. The surface chemistry of the monolayer may be affecting the surface electron density in ways not predicted by solely looking at the dielectric constant. The inset of Figure 9 illustrates the calculated shift in LSPR, $\Delta\lambda_{max}$, versus thickness of the dielectric shell. From the slope of the linear fit, Mie theory predicts that the LSPR shifts by 6 nm per every 1 nm of SAM shell. Using the estimate of a 2 nm thick shell corresponding to a monolayer of 1-HDT, we find that the predicted LSPR shift is about 0.75 nm per carbon atom. The sensitivity we observe experimentally is approximately a factor of 4 greater than this Mie theory prediction. It should also be noted that the same calculations presented in Figure 9 were also performed on Ag cores with radius = 97 nm so that the λ_{max} of the extinction would be in approximately the same region as the NSL-fabricated nanoparticles. The extent of the calculated SAM-induced LSPR shift for the larger particles was the same as what was observed for the smaller Ag cores.

The extinction was also calculated for a Ag nanosphere with a 2 nm thick shell of $n = 1.42$ for various values of $n_{external}$ to simulate a 1-HDT modified nanoparticle in various solvents as displayed in Figure 8. Similar calculations were also performed on a Ag nanosphere with no dielectric shell. Figure 10 shows the calculated peak shift, $\Delta\lambda_{max}$, versus $n_{external}$ for the nanosphere with and without the 2 nm dielectric shell. Similar to the experimental results, the calculated shifts increase linearly with respect to $n_{external}$ with sensitivity factors, $\Delta\lambda_{max}/\Delta n_{external}$, of 212 and 168 nm RIU^{-1} for the bare nanosphere and nanosphere with the dielectric shell, respectively. When the slopes of the two lines are compared, it appears that the sensitivity to $n_{external}$ for the shell-encapsulated sphere is roughly 20% less than that for the bare sphere. This degree of attenuation in the sensitivity is in excellent agreement with the experimental results shown in Figure 8. Comparing the absolute sensitivity factors for the calculated extinction to those measured experimentally, we find that the calculated sensitivity is slightly larger (212 nm RIU^{-1} calculated vs 191 nm RIU^{-1} experimental). This discrepancy can be explained by the fact that only 72% of the nanoparticle's surface area is exposed to solvent in the experiment due to the presence of the substrate.

Mie theory calculations have been carried out previously[80] for a 30 nm radius silver sphere and a mica shell of variable thickness to verify that the LSPR wavelength shift saturates for a shell thickness of ~60 nm (see Figure 5a, ref 80). A plot of the LSPR shift as a function of shell thickness, t_{shell}, is reasonably well described by:

$$\Delta\lambda_{max} = a(1 - \exp(-t_{shell}/l_d)) \quad (1)$$

where $a = 120$ nm (the LSPR shift in the limit of large shell thickness) and $l_d = 20$ nm (the characteristic decay length of the electromagnetic field surrounding the nanoparticle). The inset to Figure 9 represents the limit of small t_{shell} where the exponential reduces to a linear function. As a result of these calculations, we conclude that the electromagnetic fields of the LSPR penetrate into the adjacent solution layer ~50−60 nm

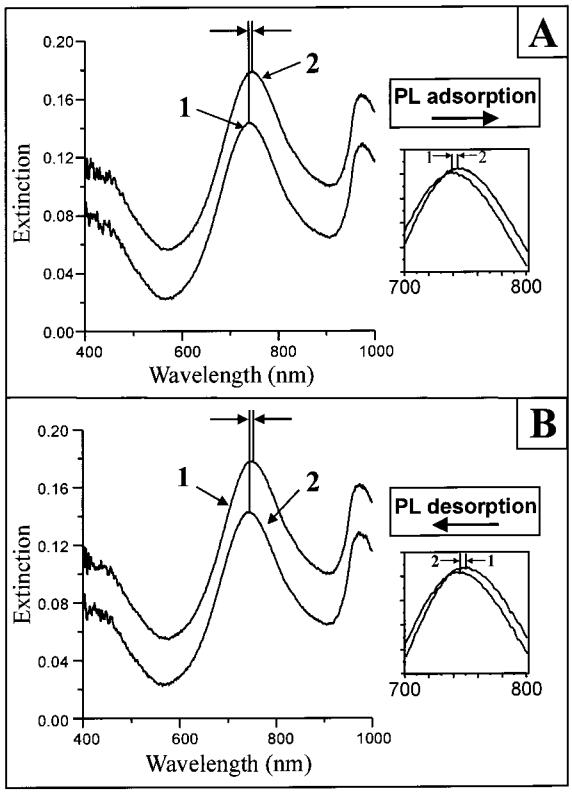

Figure 11. LSPR detected absorption/desorption of PL to 11-MUA/1-OT mixed SAM. (A) PL adsorption: (1) Extinction spectrum of 11-MUA/1-OT modified Ag nanoparticles ($D = 400$ nm, $d_m = 50$ nm) in 5 mM phosphate buffer, pH 8.5; $\lambda_{max} = 744.6$ nm. (2) Extinction spectrum after incubation with PL (1 mM in lysine); $\lambda_{max} = 749.8$ nm. (B) PL desorption: (1) Extinction spectrum of 11-MUA/1-OT modified Ag nanoparticles with adsorbed PL in 5 mM phosphate buffer, pH 8.5; $\lambda_{max} = 749.8$ nm. (2) Extinction spectrum after introducing high ionic strength buffer (20 mM phosphate buffered saline; 278 mM NaCl; 5.7 mM KCl); $\lambda_{max} = 744.9$ nm.

and, therefore, are potentially sensitive to analyte binding events at the SAM/aqueous solution interface.

LSPR Detection of Binding Events to Functionalized SAM. The results shown in Figure 8 suggested that LSPR could be used to measure changes in refractive index induced by analyte binding events to Ag nanoparticles modified with functionalized SAMs. We chose to study the binding of the multiply charged polypeptide poly-L-lysine (PL) to a mixed monolayer of 11-mercaptoundecanoic acid (11-MUA) and 1-octanethiol (1-OT). In this well-characterized model system,[92−94] the positively charged ammonium groups from the lysine residues electrostatically bind to the negatively charged surface provided by the deprotonated carboxylic acid groups from the 11-MUA. Dilution of the 11-MUA monolayer with a shorter methyl-terminated alkanethiol promotes ionization of the COOH headgroup by eliminating steric hindrance and preventing hydrogen bonding between neighboring end groups. Figure 11A-1 displays the LSPR extinction spectrum for Ag nanoparticles modified with 1:3 11-MUA:1-OT in 5 mM phosphate buffer at pH 8.5. In this pH range, the carboxylate groups on the surface and the ammonium groups in the polypeptide side chains should be in oppositely charged states, making the formation of ion pairs possible. Figure 11A-2 shows the

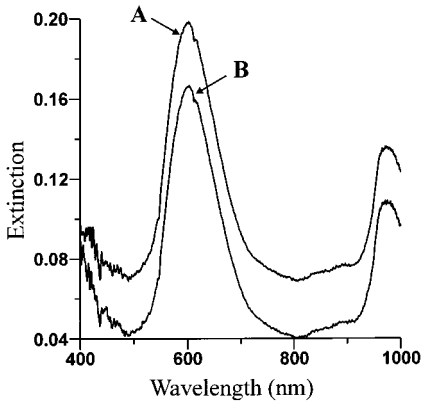

Figure 12. Lack of nonspecific binding of PL to unmodified Ag nanoparticles: (A) Extinction spectrum of Ag nanoparticles ($D = 400$ nm, $d_m = 50$ nm) in 5 mM phosphate buffer, pH 8.5; $\lambda_{max} = 602$ nm. (B) Extinction spectrum after incubation of PL in 5 mM phosphate buffer, pH 8.5; $\lambda_{max} = 602$ nm. PL solution was 1 mM in lysine residue.

extinction spectrum after PL (1 mM in lysine) was introduced into the cell and allowed to incubate. Upon exposure to PL, λ_{max} shifts to the red 5.2 nm from 744.6 to 749.8 nm. We ascertain that this shift is the result of the PL electrostatically binding to the 11-MUA/1-OT modified Ag nanoparticles. To force PL to desorb from the nanoparticles, high ionic strength buffer (20 mM phosphate buffered saline; 278 mM NaCl, 5.7 mM KCl) was introduced into the cell to screen the ion pair formation. Figures 11B-1,B-2 show the extinction spectrum of the PL modified nanoparticles before and after incubation with the high ionic strength buffer. After exposure to high salt buffer, λ_{max} shifts to the blue 4.9 nm, from 749.8 to 744.9 nm. The blue shift upon PL desorption is nearly equal to the red shift upon PL adsorption. This indicates that the nanoparticles can be regenerated after a sensing episode. This type of reversibility is an imperative element of biosensing. Nonspecific binding is another problem that plagues many biosensing applications. To prove that what we were observing was indeed PL adsorption to the negatively charged monolayer, and not nonspecific binding, we measured the change in extinction when PL solution was allowed to incubate with unmodified nanoparticles. Figure 12 illustrates how the extinction does not change when the unmodified nanoparticles are exposed to a solution of PL.

As shown in Figure 11, the magnitude of the LSPR nanosensor response to the reversible binding of a monolayer of PL to 11-MUA/1-OT modified Ag nanoparticles is a wavelength shift, $\Delta\lambda_{max} = 5$ nm. This response is primarily a consequence of the linear dependence (Figure 8) of $\Delta\lambda_{max}$ on the change in the local refractive index of the external medium, $\Delta n_{external}$, caused by electrostatic adsorption of PL. This binding event displaces the layer of aqueous buffer with refractive index, $n_{H_2O} = 1.33$, at the SAM/Ag interface and produces a PL shell with refractive index, n_{PL}, and thickness, t_{PL}, surrounding the SAM modified Ag nanoparticle. Assuming that n_{PL} is equivalent to its bulk value of 1.52[92] and t_{PL} is large compared to the characteristic decay length of the LSPR, $l_d \sim 20$ nm, we would expect the LSPR wavelength shift to be given by:

$$\Delta\lambda_{max} = m(n_{PL} - n_{H_2O}) \qquad (2)$$

where m is the slope of Figure 8B, $\Delta\lambda_{max}/\Delta_{external} = 150$ nm RIU^{-1}. Inserting the appropriate values into eq 2, one estimates the LSPR nanosensor response to be $\Delta\lambda_{max} = 28.5$ nm, which is approximately six times the observed value. However, if $t_{PL} = 1.05 \pm 0.17$ nm as was found in the propagating SPR study

(92) Jordan, C. E.; Frey, B. L.; Kornguth, S.; Corn, R. M. *Langmuir* **1994**, *10*, 3642−3648.
(93) Frey, B. L.; Jordan, C. E.; Kornguth, S.; Corn, R. M. *Anal. Chem.* **1995**, *67*, 4452−4457.
(94) Frey, B. L.; Corn, R. M. *Anal. Chem.* **1996**, *68*, 3187−3193.

of the binding of PL to MUA/Au surfaces by Corn,[92] the thickness of the PL shell is much smaller than the characteristic decay length of the LSPR evanescent field, $l_d \sim 20$ nm, estimated by Mie theory. Consequently, eq 2 must be modified to include the LSPR distance dependence:

$$\Delta\lambda_{max} = m(n_{PL} - n_{H_2O})[1 - \exp(-t_{PL}/l_d)] \quad (3)$$

In the limit where $t_{PL} < l_d$ that applies here, eq 3 reduces to

$$\Delta\lambda_{max} = m(n_{PL} - n_{H_2O})(t_{PL}/l_d) \quad (4)$$

so that one estimates the LSPR nanosensor response to be $\Delta\lambda_{max} \sim 1.4$ nm. This estimate is consistent with the small observed value $\Delta\lambda_{max} = 5$ nm but is a factor of 3−4 low. The origin of this discrepancy is likely due to the uncertainties in our knowledge of t_{PL} and l_d. For example, it is entirely possible that $t_{PL} \sim 1.5$ nm for electrostatic adsorption of PL on Ag nanoparticles as compared to flat Au surfaces.[92] Similarly, l_d could be as small as 10 nm for the triangular Ag nanoparticles used in these experiments as compared to the value of $l_d \sim 20$ nm estimated from Mie theory on spherical Ag nanoparticles. Increasing the PL layer thickness to $t_{PL} = 1.5$ nm and decreasing the LSPR decay length to $l_d = 10$ nm gives an estimated LSPR nanosensor response of $\Delta\lambda_{max} \sim 4.3$ nm, which is in close agreement with experiment. Further experimental and theoretical efforts are required to refine our understanding of the LSPR nanosensor response.

From a practical applications perspective, some additional comments need to be made with respect to the operating lifetime of the nanosensor. The two major factors that control its lifetime are nanoparticle adhesion to the substrate in the presence of flowing aqueous buffer and chemical degradation of the nanoparticle surface. It is true that for some Ag nanoparticle/substrate samples, the nanoparticles separate from the substrate within minutes of exposure to aqueous buffer. Other samples are more robust and last hours to days. This situation needs to be dramatically improved as we transition the LSPR nanosensor from the present proof-of-concept stage to the practical implementation stage. Two strategies are in development: (1) the use of Cr or Ti adhesion layers to improve the adhesion of Ag nanoparticles to the substrate and (2) a new NSL nanofabrication scheme that allows for imbedding the Ag nanoparticles into the substrate at a controlled depth while maintaining access of the target analyte to an adequate fraction of the nanoparticle surface. At present we know that the SAM-modified Ag nanoparticles resist surface oxidation for a few days. We have not yet carried out extended lifetime testing since the adhesion problem discussed above is usually the limiting factor.

V. Conclusions

The principal discovery we report here is that the peak extinction, λ_{max}, of the LSPR of NSL-fabricated Ag nanoparticles is extraordinarily sensitive to the presence of adsorbed molecules. As part of this investigation, we first observed that the nanoparticles undergo structural changes when exposed to various solvents. The two primary structural consequences of solvent exposure included (1) increases in nanoparticle height and (2) edge-annealing of the nanoparticles' triangular tips. The combination of these two effects shifted the λ_{max} of the LSPR to the blue nearly 100 nm. For alkanethiol adsorbates, $CH_3(CH_2)_xSH$, of varying chain length, x, we discovered the following new features: (1) λ_{max} of the LSPR linearly shifts to the red 3 nm for every carbon atom in the alkane chain; (2) spectral shifts as large as 40 nm are caused by only 60 000 alkanethiol molecules per nanoparticle, which corresponds to only 100 zmol of adsorbate; and (3) the nanoparticles' sensitivity to bulk external environment is only attenuated by 20% when the nanoparticles are modified with 1-HDT (C_{15}), the longest chain alkanethiol.

Mie theory was used to calculate extinction spectra of Ag nanospheres with dielectric shells that imitated an alkanethiol SAM in both thickness and refractive index. For these calculations, the volume of the Ag nanosphere was approximately the same as that of the NSL-fabricated Ag nanoparticles studied experimentally in this investigation. We found that the results of the Mie theory on the core−shell nanospheres underestimated the experimentally observed LSPR sensitivity to an alkanethiol environment by approximately a factor of 4. This large discrepancy between theory and experiment can primarily be attributed to the inability of Mie theory to accommodate shapes other than spheres and to account for chemical changes in nanoparticle surface electronic structure caused by chemisorption of molecules. However, we found good correlation between theory and experiment when Mie theory was used to predict the level of attenuation in the sensitivity to bulk environment for nanoparticles encapsulated in a dielectric shell similar to an alkanethiol. Despite its limitations, we conclude that Mie theory is a useful tool for the study of more complicated nanoparticle systems because it can correctly predict trends in the optical properties without cumbersome calculations.

Finally, we demonstrated that we have created a new class of nanosensors. Analyte binding events to Ag nanoparticles modified with functionalized SAMs should produce changes in the nanoparticle's local dielectric environment and in turn produce a shift in the LSPR λ_{max}. We demonstrated this concept by electrostatically binding the cationic polypeptide PL to nanoparticles modified with deprotonated carboxylate groups from 11-MUA. Under buffer conditions, we found that the LSPR shifted to the red 5 nm when PL was adsorbed to the modified particles and reversibly shifted back when PL was desorbed by the introduction of salt to screen the electrostatic attractions. Furthermore, we established that this system did not exhibit detectable nonspecific binding. No shift in the LSPR was measured when PL was introduced to Ag nanoparticles not modified with negatively charged SAM. Reversibility and lack of nonspecific binding are two key elements required of successful biosensors.

It is important to point out here that the LSPR nanosensors described above, while having excellent sensing capabilities, are not as intrinsically sensitive as the widely applied propagating SPP biosensor. The most direct comparison is afforded by the work of Yee and co-workers who quantitatively investigated the response of a collimated, white light, fixed angle SPP sensor and showed sensitivity factors of ∼3100 to 8800 nm RIU^{-1}.[91] Thus the propagating SPP sensor can be 20−60 times more sensitive than the LSPR nanosensor described here with a sensitivity of ∼150 nm RIU^{-1}. Nevertheless, the LSPR nanosensor has at least three unique properties in comparison to the SPP biosensor. First, the rate of analyte mass transport to a nanoparticle sensor will be governed by radial diffusion and consequently will be approximately 1000 times faster than that to planar format SPP sensors operating under semi-infinite linear diffusion.[95] The faster response times of nanoparticle sensors should permit kinetic binding studies of macromolecular target

(95) Wightman, R. M.; Wipf, D. O. *Voltammetry at Ultramicroelectrodies*; Allen, J. B., Ed.; Marcel Dekker: New York and Basel, 1989; Vol. 15, pp 267−353.

analytes that are not currently possible. Second, LSPR nanosensor arrays will provide pixel sizes 20 to 50 times smaller than the SPP sensor arrays due to the 2−5 μm length scale of SPP propagation.[34] Third, these Ag nanoparticle sensors will simultaneously exhibit LSPR shifts and surface-enhanced Raman scattering (SERS). Thus, the potential exists for rapid, high-throughput screening of binding events with extremely simple instrumentation followed by analyte identification, perhaps even at the single molecule level, with SERS. Therefore, we believe that nanoparticle sensors, as we describe here, will have a profound impact on new chemosensor and biosensor technologies in environmental and biological applications as well as in exploring the information content inherent in molecular recognition events.

Acknowledgment. Funding was provided by the ARO (Grant DAAG55-97-1-0133), NSF (Grant CHE-940078), and the MRSEC program of the NSF (Grants DMR-9632472 and DMR-0076097).

JA003312A